Steered Molecular Dynamics Simulations on the "Tail Helix Latch" Hypothesis in the Gelsolin Activation Process

Feng Cheng, Jianhua Shen, Xiaomin Luo, Hualiang Jiang, and Kaixian Chen
Center for Drug Discovery and Design, State Key Laboratory of Drug Research, Shanghai Institute of Materia Medica, Shanghai Institutes for Biological Sciences, Chinese Academy of Sciences, 294 Taiyuan Road, Shanghai 200031, Peoples Republic of China

ABSTRACT The molecular basis of the "tail helix latch" hypothesis in the gelsolin activation process has been studied by using the steered molecular dynamics simulations. In the present nanosecond scale simulations, the tail helix of gelsolin was pulled away from the S2 binding surface, and the required forces were calculated, from which the properties of binding between the tail helix and S2 domain and their dynamic unbinding processes were obtained. The force profile provides a detailed rupture mechanism that includes six major unbinding steps. In particular, the hydrogen bonds formed between Arg-207 and Asp-744 and between Arg-221 and Leu-753 are of the most important interaction pairs. The two hydrogen bond "clamps" stabilize the complex. The subsequent simulation on Arg-207-Ala (R207A) mutation of gelsolin indicated that this mutation facilitates the unbinding of the tail helix and that the contribution of the hydrogen bond between Arg-207 and Asp-744 to the binding is more than 50%, which offers a new clue for further mutagenesis study on the activation mechanism of gelsolin. Surrounding water molecules enhance the stability of the tail helix and facilitate the rupture process. Additionally, temperature also has a significant effect on the conformation of the arginine and arginine-related interactions, which revealed the molecular basis of the temperature dependence in gelsolin activation.

INTRODUCTION

The actin-binding protein gelsolin is involved in remodeling of the cytoskeleton during growth-factor signaling, apoptosis, cytokinesis, and cell movement. In the presence of calcium ion, gelsolin is activated and severs assembled actin filaments in two parts, then caps the fast-growing plus end of a free or newly severed filament, which leads to cytoskeletal destruction and cell shape changes (Kwiatkowski, 1999; Lin et al., 2000; McGough, 1998; Robinson et al., 1999; Sun et al., 1999). Recent evidence also shows the important roles that gelsolin plays in neurite filopodial retraction, neuronal ion channel modulation, and phosphoinositide signaling regulation (Kwiatkowski, 1999; Sun et al., 1999). In addition, gelsolin appears to be important in carcinogenesis (Kwiatkowski, 1999; Sun et al., 1999). Therefore, studying the activation mechanism of gelsolin is of significance in understanding signaling transduction, cell apoptosis, and the treatment of cancers.

Gelsolin has two tandem homologous halves, each contains a threefold segmental repeat, segments S1–S3 (N-half) and S4–S6 (C-half), respectively (Kwiatkowski et al., 1986; Robinson et al., 1999; Sun et al., 1999; Way and Weeds, 1988) (Fig. 1). The C-half acts as a regulatory domain to control the activity of gelsolin. The N-half severs actin filament by binding along the sides of actin filament through S2 site only if Ca^{2+} ion induces a conformational change in the C-half to expose the actin-binding site S2 (Kwiatkowski et al., 1989; Lin et al., 2000; Sun et al., 1999). Experiments show that it takes at least 10^{-6}M Ca^{2+} to "open up" the C-half from the N-half at room temperature (Bryan, 1988; Chaponnier et al., 1986; Lin et al., 2000). Remarkably, deletion of just 23 residues (Phe-733–Ala-755) from the C terminus allows gelsolin to sever in the absence of Ca^{2+} (in EGTA) (Kwiatkowski et al., 1989; Lin et al., 2000). These results provide the indication that these residues play a major role in the regulation of the C-half. The three-dimensional crystal structure of the full-length gelsolin (Burtnick et al., 1997) (Fig. 1) shows that these 23 residues are part of the S6 tail (Phe-732–Ala-755). This tail contains a proximal unstructured strand that is capped at the C terminus by a short helix (Asp-744–Ala-755). The tail helix is closely aligned with the S2 actin-binding site. Therefore, this helix has been postulated to serve as a latch to block S2 from binding to actin and to keep gelsolin inactive (Burtnick et al., 1997; Lin et al., 2000; Sun et al., 1999); the regulation of the C-half is practiced by the specific interaction between the S6 tail helix and S2 and the tail helix unlatching is the most critical step in the gelsolin activation process. This is called "tail helix latch" hypothesis (Burtnick et al., 1997; Lin et al., 2000; Lueck et al., 2000; Sun et al., 1999).

The "tail helix latch" hypothesis was firstly proposed based on the x-ray crystal structural data by Burtnick and his colleagues (Burtnick et al., 1997). The importance of tail helix in maintaining the inactive gelsolin conformation was further verified by biochemical experiments (Lin et al., 2000; Lueck et al., 2000; Pope et al., 1997; Selden et al., 1998). Despite progress in research on the specific binding between tail helix and S2, it is little known about the molecular basis for "tail helix latch" mechanism and for the

Submitted January 5, 2002, and accepted for publication March 26, 2002.
Address reprint requests to Profs. Hualiang Jiang and Jianhua Shen, Shanghai Institute of Materia Medica, Chinese Academy of Sciences, 294 Taiyuan Road, Shanghai; 200031, P. R. China. Tel.: 86-21-64318401; Fax: 86-21-64370269; E-mail: jiang@iris3.simm.ac.cn or jhshen@mail.shcnc.ac.cn.

0006-3495/02/08/753/10 $2.00

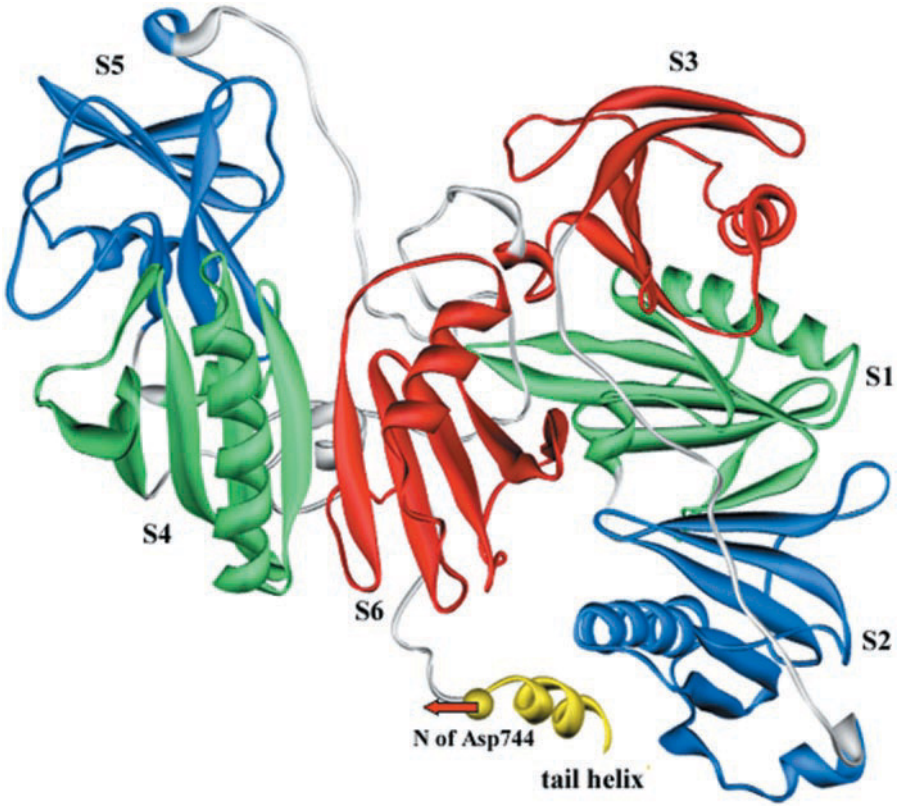

FIGURE 1 Solid ribbons scheme of the crystal structure of the full-length equine plasma gelsolin in its inactive state. S1∼S6 represent six gelsolin segments. The tail helix (*yellow*), linking with S6, contacts S2. The yellow ball is the backbone N atom of Asp-744, to which the harmonic potential is assigned, and the red arrow is the moving direction of the tail helix in the SMD simulations (Fig. 2).

dynamic tail-helix-unlatching pathway. To explore the microscopic dynamic processes of tail helix unlatching and to provide new insights into this hypothesis, a steered molecular dynamics (SMD) simulation study was performed. In the present computational simulations, the tail helix is pulled away from the S2, and the required force was calculated, from which both binding characteristics and the dynamic unbinding processes were obtained. In this way, the molecular basis of the tail helix latch hypothesis has been well explained.

In this paper, three models have been presented to describe the tail helix unlatching process in different situations, of which models 1 (Fig. 2) and 3 were chosen to simulate the tail-S2 complex in water and vacuum, respectively; and in model 2, the Arg-207-Ala (R207A) mutation was simulated in water solution to probe the role of Arg-207 in the gelsolin activation. First, the optimal pulling velocity was chosen, and the rupture force was extrapolated. The subsequent rupture force profile analysis based on this suitable velocity suggests a detailed tail helix unlatching mechanism involving several major unbinding steps. The virtual mutation of R207A was performed, and the SMD simulation indicates that this mutation facilitates the unbinding of tail helix, and the contribution of the hydrogen bond between Arg-207 and Asp-744 to the binding is more than 50%. In the rupture process, water molecules enhance the stability of the tail helix and are helpful to unbinding of the tail helix from S2. Finally, the molecular basis of the temperature dependence of the gelsolin activation was also presented.

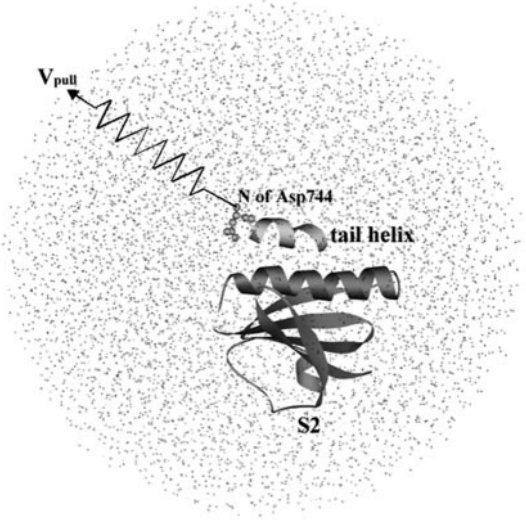

FIGURE 2 Ribbon schematic representations of solvated tail-S2 model 1. The dot points represent the water molecules. During the SMD simulation, the tail helix is pulled away from S2 through a harmonic potential (symbolized by an artificial spring) that is connected to the Asp-744 backbone nitrogen atom (Fig. 1). This pulling potential moves with a constant velocity V_{pull} (*arrow*). The direction of spring is donated as z axis.

MATERIAL AND METHODS

Molecular models

The vacuum tail-S2 model (model 3) were constructed based on the x-ray crystallographic structure of the calcium-free equine plasma gelsolin taken from the Brookhaven Protein Data Bank (Bernstein et al., 1977), entry 1d0n. The resolution of this structure is 2.50 Å. The whole tail helix (residues from Asp-744–Ala-755) and S2 (residues from Val-158–Leu-247) were included in the simulations.

The solvated tail-S2 model (model 1) was constructed based on model 3. First, it was built by surrounding model 3 with a sphere droplet containing 8095 TIP3 (Jorgensen, 1981; Neria et al., 1996) water molecules using the program SOLVATE developed by Prof. Grubmüller. The radius of the water droplet was 40 Å, which ensures the whole protein surface to be covered by water molecules at least 12 Å thick. Next, restraints were added to the solvated system. All molecules in a surface layer of 6 Å thick were subjected to SBOUND forces (Brooks and Karplus, 1983), which counterbalance surface tension and evaporation, and thus restrain the water molecules to a given volume. The tail-S2 protein complex was placed in the lower part of the droplet, thus the tail helix has enough moving space, which prevents it from entering the 6-Å restraint region during the whole simulation process. Moreover, the center of mass of the S2 was fixed by adding a stiff harmonic potential to avoid the movement of S2, thereby the tail-helix-unbinding process can be detected clearly and the rupture force can be computed correctly.

Virtual mutation of Arg-207-Ala for model 3 was performed by using molecular modeling software, SYBYL Release 6.7 (Tripos Inc., St. Louis, MO). This mutated model was then solvated by using the same process as model 1, which resulted model 2.

SMD simulation

The MD simulations were performed with the parallel MD program EGO, in which the CHARMM19 force field (Brooks et al., 1983) is adopted. All simulations were carried out with an integration step size of 10^{-15} s. The lengths of chemical bonds involving hydrogen atoms are fixed with SHAKE algorithm (Brooks and Karplus, 1983).

To obtain a starting point for the SMD simulations, both the solvated and vacuum models were minimized using the minimization routine of EGO. Briefly, the atom velocities were rescaled by a friction factor τ of 0.1 at the end of each integration step, and the maximal position movement per integration step for atoms was set up to be no more than 0.08 Å. As a result of such a minimization procedure the simulation system constantly looses energy until the system stays in a local structural minimum at temperature 0 K. A measure the simulation system apart from a local minimum was given by the maximal force and the average force of all atoms. The maximal force was set as 20 kcal/(mol·Å) for model 3, and 100 kcal/(mol·Å) for models 1 and 2; the average force of was set as 1.5 kcal/(mol·Å) for model 3 and 20 kcal/(mol·Å) for models 1 and 2. After the structural minimization convergence was reached, model 3 was directly coupled to a heat bath of 298 K by velocity rescaling with a coupling constant of 10^{-13} s^{-1}; and the structure was kept equilibrium at this temperature for 1.0 ns. To correct some structural conflicts possibly existing between water molecules and the protein in models 1 and 2, the solvated models were heated up to 298 K over 10 ps, the systems were then equilibrated at 298 K for 190 ps. During this process, the water molecules were relaxed and the protein was restrained to its original position. Next, removing the constraints on the protein, the models were subjected to a free 1.0-ns dynamics calculation, ensuring the whole system to be equilibrated.

Once the equilibrated systems were obtained, the subsequent SMD simulations were performed. The tail helix was pulled away from the S2 subunit by subjecting an artificial harmonic potential as shown by the symbolic "spring" in Fig. 2. In the activation process of gelsolin, calcium binding induces the S6 subunit a large conformational change and movement (Robinson et al., 1999), which lead to the unbinding of the tail helix from the S2 subunit (actin binding site). As shown in Fig. 1, the backbone nitrogen atom (N) in Asp-744 of the N terminus of the tail helix links with the gelsolin S6 subunit, thus the influence resulted from the conformational change and movement of S6 may transfer to the tail helix through this N atom. We therefore assigned the pulling potential to the N atom of Asp-744 to simulate the conformational change and movement of the S6 subunit. The harmonic potential was oriented toward the direction the tail helix moving along with the S6 movement (Figs. 1 and 2).

All SMD simulations began with an equilibrated protein structure and ended when the tail helix was completely ruptured from S2. During the enforced unbinding, the energy of the system and the pulling force acting on the N atom of Asp-744 were calculated and recorded every 10 fs, and the structure was recorded per 1 ps.

RESULTS AND DISCUSSIONS

Equilibrium

In this section we provide evidence that our system preparation resulted in a properly equilibrated protein. System temperature, total energy, and the heavy atom root-mean-square deviations from the x-ray structure ($rmsd_{x\text{-}ray}$) are three important criterions for the convergence of the protein system. These properties of the three simulation models versus simulation time are shown in Fig. 3, which indicates that the system temperatures of the three models keep in constant during the simulations and the total energies have been stable after 700 ps equilibration. The $rmsd_{x\text{-}ray}$ of vacuum model 3 increases sharply from 0 to 4 Å in the first 5-ps equilibration and then keeps almost stable. For the $rmsd_{x\text{-}ray}$ values of models 1 and 2, it takes 600 ps to reach stability because of the large size of the aqueous models. These results show that after 1.0-ns MD simulation, the three models are equilibrated and then the systems can be used as the starting points for the further SMD simulations.

Choice of the pulling velocity

The pulling velocity (V_{pull}) is an important parameter in the SMD simulations. The simulations at higher pulling velocity may lead to remarkable nonequilibrium effects and relaxation of the tail helix, which may introduce obvious errors to the simulation results (Isralewitz et al., 2001). The low-velocity SMD simulations that carried out on a millisecond time scale can overcome these disadvantages and reproduce actual atomic force microscopy experiments, however, the corresponding computational cost will be very expensive. To find an optimal simulation velocity, a process similar in the streptavidin-biotin binding simulation carried out by Grubmüller et al. (1996) was used, i.e., 7 SMD simulations at different pulling velocities ranging from 0.015 Å/ps to 0.24 Å/ps have been performed on the tail-S2 systems.

Fig. 4 shows the force profile obtained from one of the SMD simulations of the solvated model 1 after 1.0-ns equilibration with pulling velocity V_{pull} = 0.015 Å/ps at 298 K.

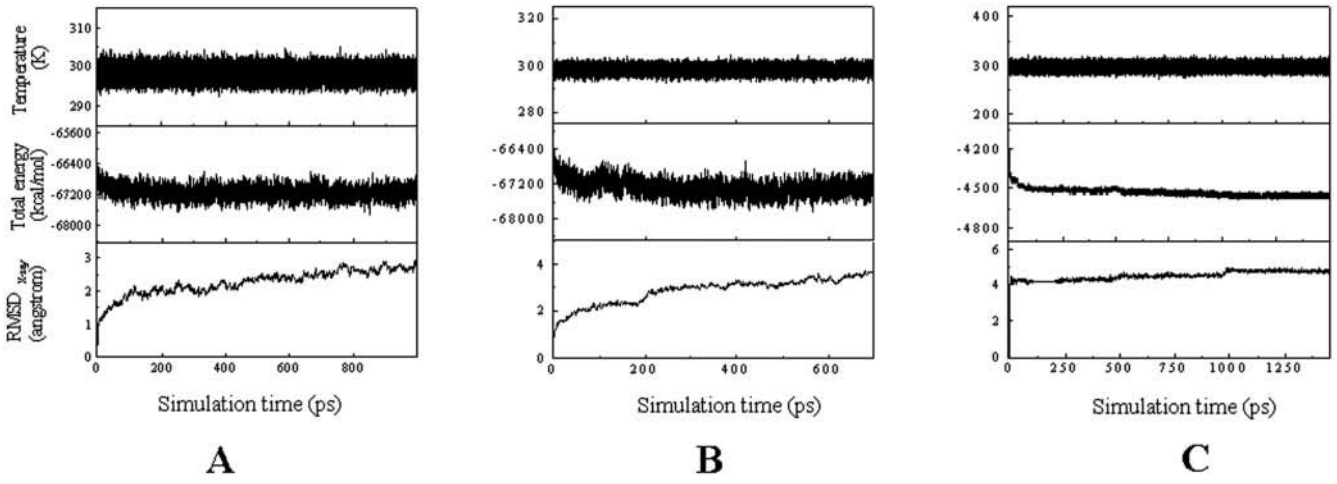

FIGURE 3 System temperature, total energy, and $rmsd_{x\text{-}ray}$ of three models versus simulation time. (*A*) Model 1; (*B*) model 2; (*C*) model 3.

The *X* coordinate axis is the external potential position $Z_{potential}$ and *Y* axis is the corresponding force. The force profile (Fig. 4 *A*) shows the fast fluctuations, which were removed by smoothing these force profiles using FFT (Fast Fourier Transform) filters with 8-ps width (Fig. 4 *B*). However, some error was brought by this method because the calculated force value is a function of the smoothing width. To evaluate this uncertainty, error bars were determined by rescaling force profiles with 4 ps width as upper bound and with 12 ps width as lower bound, respectively. This smooth and error estimation technique was adopted for all force curves throughout in the present paper.

The computed unbinding forces varied with the pulling velocity. Fig. 5 summarizes the results of the 7 SMD simulations for the solvated model 1 at different pulling velocities. Three velocity regimes can be distinguished: a "low velocity" regime below 0.09 Å/ps; an intermediate regime between 0.09 Å/ps and 0.18 Å/ps; and a "high velocity" regime above 0.18 Å/ps. The apparent linear correlation between the computed rupture force and the pulling velocity less than 0.09 Å/ps demonstrates that the friction force described by a friction coefficient of 26.2 pN s m^{-1} is dominative in the low velocity regime. With the linear fit analysis, the rupture force is extrapolated to 395 pN when the V_{pull} is approaching 0 Å/ps. In the intermediate regime, the rupture force saturates. At velocities higher than 0.18 Å/ps, the force increases again. This is because that at such large velocities, the adjustment of the tail helix to the external potential falls behind spring movement, which results in the helix uncoiled, and more force is therefore required in the high velocity regime.

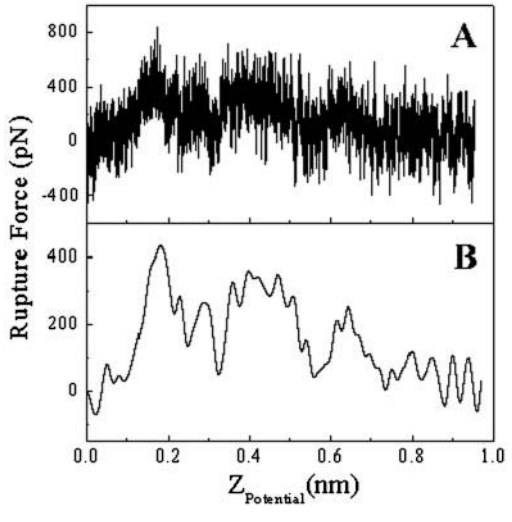

FIGURE 4 (*A*) Rupture force exerted on the tail helix of unbinding process as a function of external potential position $Z_{potential}$ at a pulling velocity of 0.015 Å/ps. (*B*) To eliminate the fast fluctuations, the pulling force was smoothed with an FFT filter of width 8 ps.

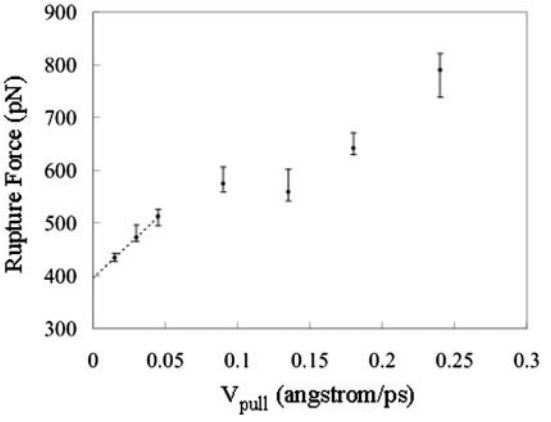

FIGURE 5 Computed rupture forces as a function of pulling velocity V_{pull}. The error bars give an estimated uncertainty. The dashed line shows a linear fit to the computed forces for V_{pull} less than 0.09 Å/ps.

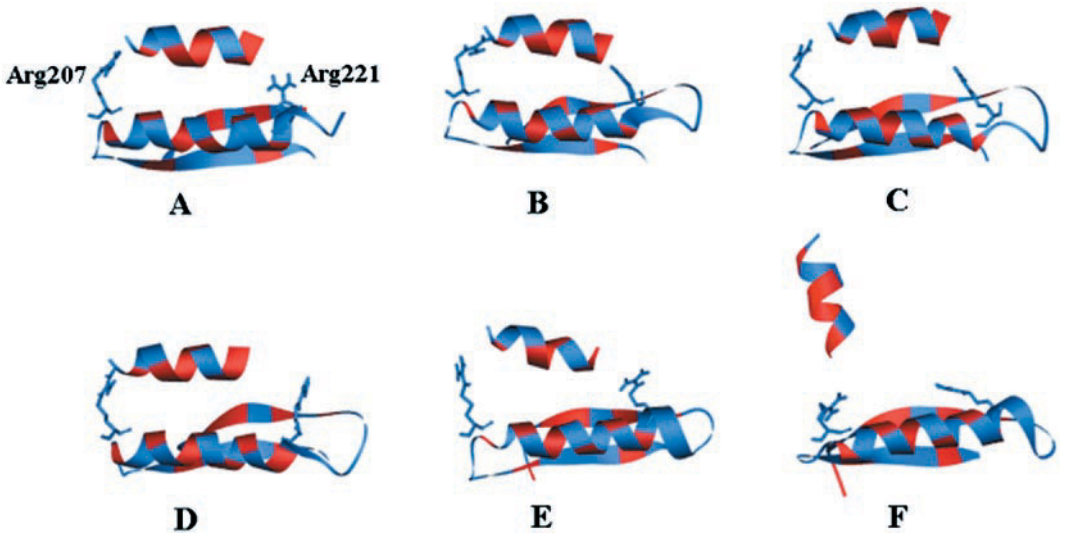

FIGURE 6 "Snapshots" of rupture. Tail helix and S2 are drawn in flat ribbon model and two important residues, Arg-207 and Arg-221, are shown in stick model. Snapshots were recorded at *A* at the start of stretching simulation ($Z_{potential}$ = 0.0 nm), (*B*) $Z_{potential}$ = 0.18 nm, (*C*) $Z_{potential}$ = 0.32 nm, (*D*) $Z_{potential}$ = 0.41 nm, (*E*) $Z_{potential}$ = 0.74 nm, and (*F*) $Z_{potential}$ = 0.90 nm.

In the present SMD simulations, the pulling velocity was chosen at 0.015 Å/ps, because on one hand at such low velocity, the external harmonic potential has no obvious influence on the structure of tail helix; on the other hand, the whole tail helix rupture simulation can be achieved in 2 weeks by using our supercomputer at this pulling velocity.

Rupture mechanism

To reveal the molecular basis of the tail helix latch hypothesis clearly, the following discussions shown as four subsections might be plausible. The initial structural analysis suggests a detailed rupture mechanism in the aqueous solution. The subsequent point mutation simulation evaluates quantitatively the contribution of a certain residue to the binding and unbinding, which provides an indirect confirmation to the rupture mechanism. Because the gelsolin activation process is sensitive to the environmental situations, the final discussion on the effects of water and temperature is necessary for a complete description of the rupture mechanism.

Structural analysis

The force peaks and troughs in the force profile obtained from the SMD simulation (Fig. 4 *B*) reflect the complexity of the unlatching process of the tail helix from S2. To explain the relationship between the calculated pulling forces and the interactions between the tail helix and S2, six "snapshots" (Fig. 6) are taken to describe major steps in the rupture process. The corresponding hydrogen bonds and hydrophobic interactions were respectively calculated by using HBPLUS (McDonald and Thornton, 1994) and LIGPLOT (Wallace et al., 1995) programs (Fig. 7).

The initial tail-helix-S2 complex (Figs. 6 *A* and 7 *A*) is stabilized by some specific hydrogen bonds and hydrophobic interactions. Three hydrogen bond pairs form between the tail helix and S2, namely, Arg-207–Asp-744, Lys-218–Glu-752 and Arg-221-Leu-753; among them Arg-207 and Arg-221 act as two hydrogen bond "clamps" grasping the tail helix. Besides hydrogen bonding interactions, hydrophobic contacts are also important. The amino acids on the bottom of the tail helix, including Leu-746, Ala-749, Leu-750, Ala-751, Leu-753, Ala-754, and Ala-755, and those on the top of the S2, Phe-208, Leu-211, Ala-213, Val-216, Ile-220, Val-231, Val-233, and Phe-234 are all hydrophobic or partial hydrophobic residues, which are colored red in Fig. 6 *A*. These residues form two hydrophobic interaction patches, which strong contact with S2 through hydrophobic interactions when spatial orientations are appropriate (Figs. 6 and 7). In the starting configuration of the stretching simulations, two hydrophobic contacts form between the tail helix and residues Arg-210 and Leu-211 (Fig. 7 *A*). After the external potential moved to $Z_{potential}$ = 0.18 nm, another hydrogen bond forms between Arg-207 and Asp-744 (Figs. 6 *B* and 7 *B*); the tail helix forms three hydrophobic contacts with Thr-214, Ser-217 and Lys-218, which not only makes up the break of the hydrogen bond between Lys-218 and Glu-752, but also effectively stabilizes the tail-S2 complex. Accordingly, the corresponding rupture force increases up to 440 pN. This point is the global maximum in the force profile (Fig. 4 *B*). With further stretching, the right "clamp," hydrogen bond between Arg-221 and Leu-753, is weakened and breaks at an extension at

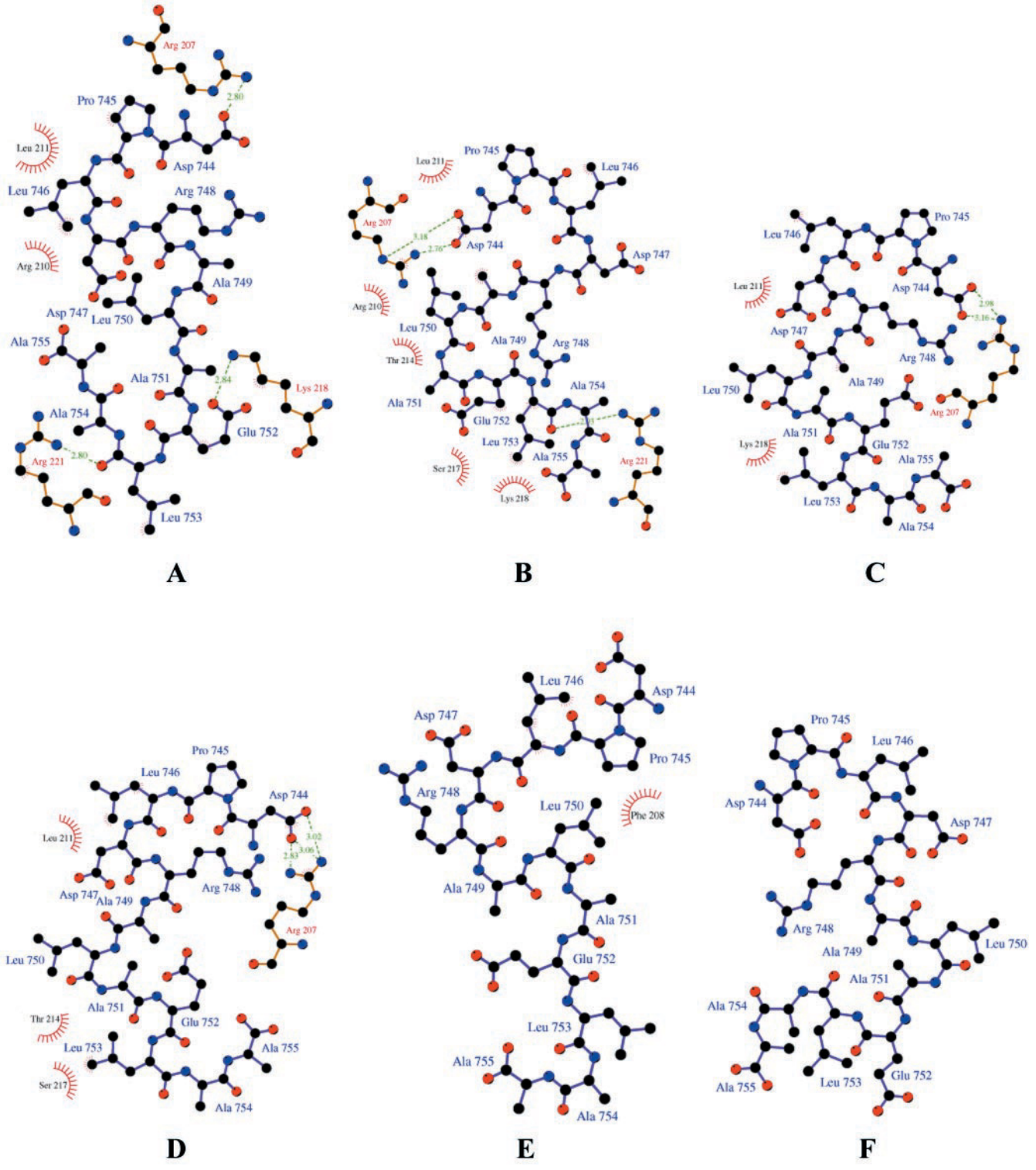

FIGURE 7 Schematic representations of hydrogen bond and hydrophobic interactions between tail helix and S2 at different stages of rupture. Snapshots were recorded at *A* at the start of stretching simulation ($Z_{potential}$ = 0.0 nm), (*B*) $Z_{potential}$ = 0.18 nm, (*C*) $Z_{potential}$ = 0.32 nm, (*D*) $Z_{potential}$ = 0.41 nm, (*E*) $Z_{potential}$ = 0.74 nm, and (*F*) $Z_{potential}$ = 0.90 nm. These figures were made with the program LIGPLOT. Dashed lines represent hydrogen bonds and spiked residues form van der Waals contacts with the tail helix.

$Z_{potential}$ = 0.32 nm (Figs. 6 *C* and 7 *C*). Meanwhile, due to the spatial orientation change, only two hydrophobic contacts of the tail helix with Lys-218 and Leu-211 survive, and thus rupture force drops rapidly to 50 pN. Further move-

ment of the helix makes Asp-744 to be close to Arg-207, the third hydrogen bond between them forms at this stage. This strengthened hydrogen bond and the subsequently established hydrophobic contacts of the tail helix with Tyr-214 and Ser-217 give rise to the second force peaks (300∼350 pN) at an extension from 0.32 to 0.54 nm (Figs. 6 *D* and 7 *D*). As the pulling process continues, the "left clamp," hydrogen bonds formed between Arg-207 and Asp-744, begins to break and the rupture force decreases accordingly. When the external potential reaches $Z_{potential}$ = 0.74 nm (Figs. 6 *E* and 7 *E*), the rupture of Arg-207–Asp-744 occurs and only one hydrophobic contact between the tail helix and Phe-208 are left. At the extension of $Z_{potential}$ = 0.90 nm (Figs. 6 *F* and 7 *F*), i.e., after 600-ps stretching simulations, the last contact breaks, and the tail helix is ruptured completely away from S2. The fluctuation of the force beyond 0.90 nm could be attributed to the interaction with solvent molecules.

Importance of Arg-207

The structure analysis provided a detailed insight into the rupture process of tail-helix-S2 complex. It attributes the rupture force to a network of hydrogen bonds and hydrophobic interactions between the tail helix and S2. In particular, it shows that the hydrogen bond formed between Arg-207 and Asp-744 is the most important interaction. To study the function of Arg-207 quantitatively, SMD simulation was performed on the R207A mutant model (model 2).

The simulation results of model 2 are summarized in Fig. 8. The conformations of models 1 and 2 after 1.0-ns equilibration are compared in Fig. 8 *A*. Apparently, without the tackle of Arg-207 "clamp," the N terminus of the tail helix departs from S2 spontaneously after the equilibration simulations. Fig. 8 *B* shows the force profile obtained from the subsequent SMD simulation for model 2 at a pulling velocity of 0.015 Å/ps. Being substituted of Arg-207 by Ala, the corresponding rupture force peak drops sharply from 440 (Fig. 4 *B*) to 200 pN. The decreased value of the unbinding force indicates that the contribution of Arg-207 to the binding of the tail helix with S2 is more than 50%. It shows quantitatively and explicitly the importance of Arg-207 during the unbinding process. This simulation gives a useful clue for the further mutation experiment: R207A mutated gelsolin might be easier to be activated because this mutation facilitates the rupture of the tail helix from S2.

Role of water

It is generally recognized that water molecules are very essential to the dynamics of protein (Brooks et al., 1988). However, how and how much water affects the tail-helix-unbinding process is still unknown. Therefore, in the present work, vacuum model 3 was chosen to probe the role of water molecules in the unlatching process.

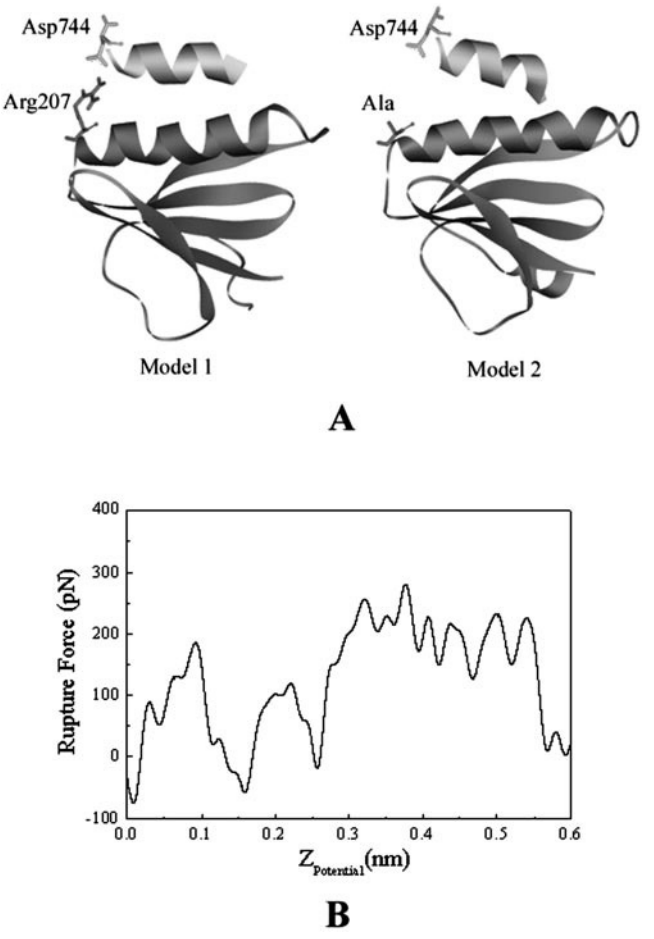

FIGURE 8 (*A*) Schematic representation of structures of models 1 and 2 after 1.0-ns equilibration. (*B*) Rupture force profile of the SMD simulation for model 2 at a pulling velocity of 0.015 Å/ps. The rupture force was smoothed by using FFT filter of width 8 ps. The tail helix and S2 are drawn in flat ribbon model and important residues are shown in stick model.

A schematic representation of conformations of model 3 in different simulation stage is shown in Fig. 9 *A*. The tail helix relaxed rapidly within the first 5 ps, which corresponds with the sharp increase of $RMSD_{x\text{-}ray}$ in Fig. 3 *C*. After 1.5-ns equilibration, the tail helix uncoiled completely. In contrast, the tail helix is well preserved in solvent (Fig. 6). This suggests that the surrounding water molecules stabilize the helix structure of the tail.

Fig. 9 *B* shows the force profile of model 3 obtained from the SMD simulation at velocity of 0.015 Å/ps. It is surprising that it takes more than 2000 pN to rupture the tail helix from S2 in vacuum. The more than 4 times increase of maximal rupture force indicates that water molecules are beneficial to the unbinding process. Water molecules may affect the unbinding process by forming hydrogen bonds with protein molecule. The unbinding process in solvent includes two steps, i.e., the rupture of interactions between

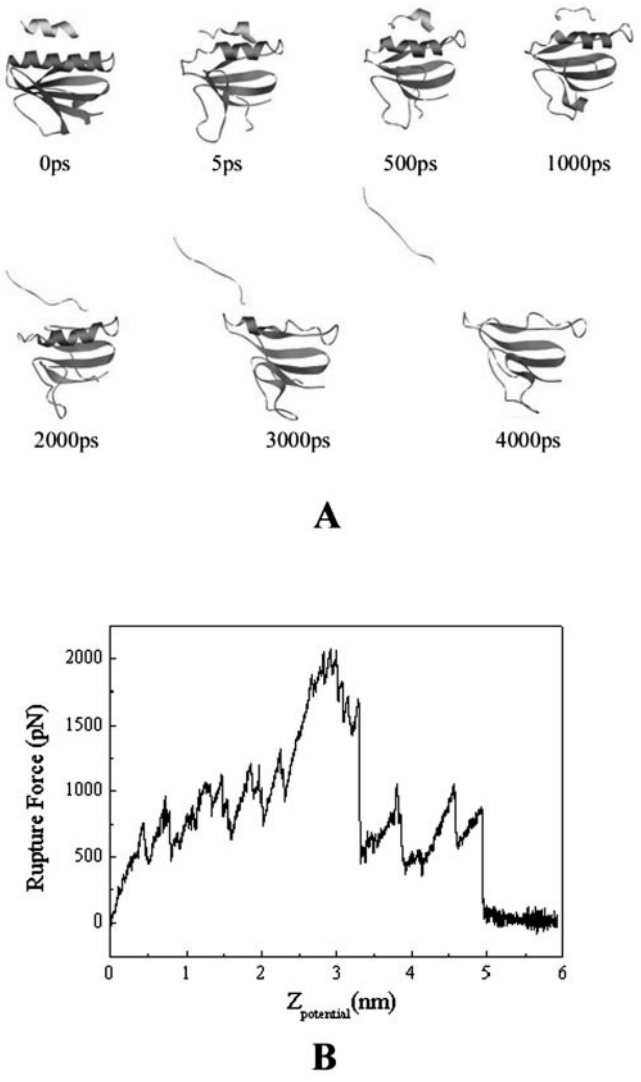

FIGURE 9 (*A*) Schematic representation of structure of model 3 in the different simulation stage in vacuum. Tail helix and S2 are drawn in flat ribbon model. (*B*) Rupture force profile of the SMD simulation for model 2 at a pulling velocity of 0.015 Å/ps. The rupture force was smoothed by using FFT filter of width 8 ps.

the tail helix and S2, and the solvation of exposed binding site. Some residues such as arginine may form new strong hydrogen bonds with surrounding water molecules when their interactions with other residues were broken. Thus, the extra solvation energy can compensate the rupture of the interactions to some extent, which may facilitate the unbinding of the complex. Therefore, it can be concluded that the solvation effect can stabilize the structure of the tail helix and can also facilitate its unbinding away from the S2 surface.

Effects of temperature

Yin's group (Lin et al., 2000) reported that Ca^{2+} activation of gelsolin severing was highly temperature dependent. Their pyrene-actin depolymerizing assay showed that at 37°C, gelsolin severing was detectable at 5×10^{-7} M, and becomes half-maximum at 2.2×10^{-6} M; whereas at 24°C the severing was not detected until at 1×10^{-5} M and was half-maximum at 1.9×10^{-5}M of Ca^{2+}. Further experiments showed that truncation of the tail helix diminished the temperature dependence of Ca^{2+} activation (Lin et al., 2000). This implies that the tail-helix-unbinding process is directly responsible for the temperature dependence in the gelsolin activation. To explore the molecular basis for this aspect, another SMD simulation for the solvated model 1 was performed at 310 K. The simulation result is shown in Fig. 10.

The rupture force profile at 310 K is shown in Fig. 10 *A*, which is very similar to that at 298 K. Notably, the maximal force decreases from 440 to 310 pN, indicating that less force is necessary for rupturing the tail helix at 310 K. This simulation is in agreement with the experiment results (Lin et al., 2000). The corresponding interaction sketch map and structure of the maxima in the force profile at 310 K are plotted in Fig. 10, *B* and *C*, respectively. By comparing Fig. 10 *B* with Fig. 7 *B*, it can be seen that, at 310 K, the major interactions such as the two hydrogen bonds between Arg-207 and Asp-744 and the hydrophobic contacts of the tail helix with Leu-211 and Thr-214 exist. Remarkable change occurs at 310 K, the "right clamp" (Fig. 6), i.e., the hydrogen bond between Arg-221 and Leu-753 and the hydrophobic contact between the tail helix and Arg-210 disappeared. This might be the reason why the rupture force is lower at 310 K than that at 298 K. Temperature has an important effect on the molecular conformation. Higher temperature may facilitate conformational rearrangements by improving the thermal motion velocity of molecule, thus energy barrier can be overcome and more stable conformations can be reached. The change of conformation is often accompanied with the variation of the interactions, which may affect the binding characteristics between two molecules. For amino acid residues, the change range of conformation depends on the size of the sidechain. Generally, with the elongation of the sidechain, the conformation change is significant and accompanied interaction variation is remarkable. Additionally, the tail helix-S2 complex is a surface-surface-binding model. Comparing the pocket-binding model, the motion of sidechains is more flexible due to less steric barrier. Therefore, in the present system, temperature has obvious influence on the arginine conformation and its related interactions, the major interactions between the tail and S2. This is the reason that why the two interactions involving arginine residue exhibit a great change when the system temperature increases from 298 to 310 K.

CONCLUSIONS

The present SMD simulations have provided a new insight into the "tail helix latch" hypothesis of gelsolin activation at

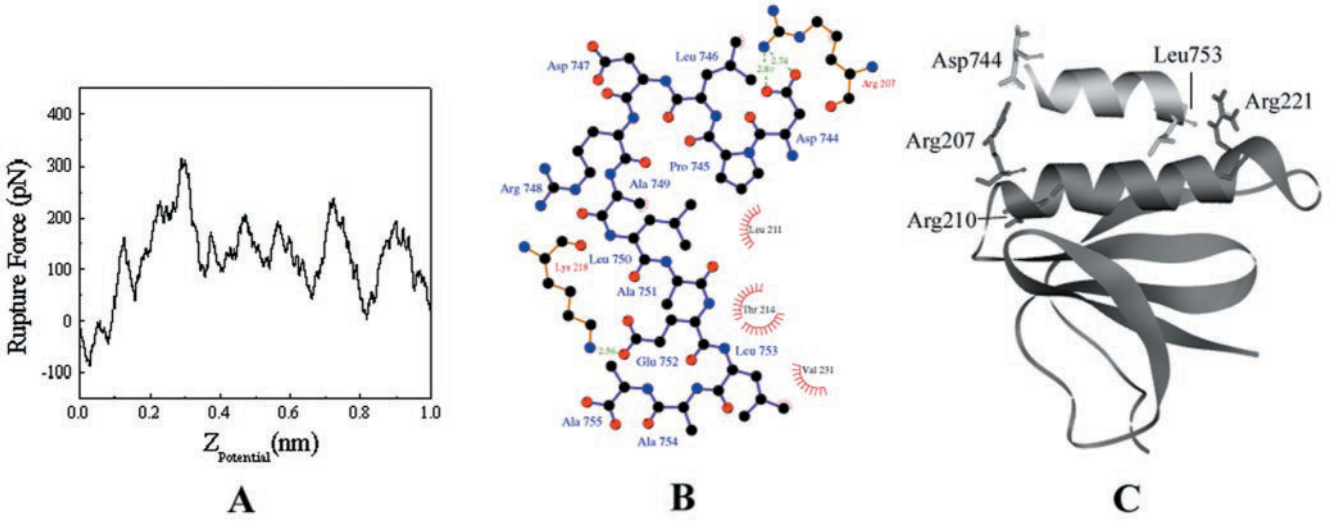

FIGURE 10 (*A*) Rupture force profile of the SMD simulation for model 1 at 310 K. The rupture force was smoothed by using FFT filter of width 8 ps. (*B*) Schematic representations of hydrogen bond and hydrophobic interactions between tail helix and S2 for model 1 at an extension of 0.30 nm (the peak of the force profile) at 310 K. This figure was made with the program LIGPLOT. Dashed lines represent hydrogen bonds and spiked residues form van der Waals contacts with the tail helix. (*C*) "Snapshot" of the structure of model 1 at an extension of 0.30 nm at 310 K. Tail helix and S2 are drawn in flat ribbon model and important residues are shown in stick model.

the atomic level. In the nanosecond simulations, the tail helix of gelsolin was pulled away from the S2 subunit, and the unbinding force required for rupturing the tail helix away from S2 was obtained. In the SMD simulations, the unbinding forces of the complex have been determined as a function of pulling velocity. The optimal pulling velocity was chosen at 0.015 Å/ps. Taking into account the frictional forces, a linear model was used to extrapolate the unbinding forces, which was calculated as 395 pN in aqueous solution. The force profile provides a detailed rupture mechanism involving six major unbinding steps. The peaks and troughs in the force profile can be assigned to the formation and rupture of specific hydrogen bonds and hydrophobic contacts. In particular, the hydrogen bond between Arg-207 and Asp-744 is the most important interaction to the rupture process. The SMD simulation on the R207A mutation model (model 2) demonstrated that the contribution of this hydrogen bond to the binding is more than 50%. Water molecules enhance the stability of the tail helix and facilitate the rupture of the complex. Temperature also has a significant effect on the conformation of the arginine and arginine-related interactions. This may be the molecular basis of the temperature dependence in gelsolin activation.

The authors would like to thank Dr. Helmut Grubmüller for his kindness in offering the EGO program. We gratefully acknowledge financial support from National Natural Science Foundation of China (grants 29725203 and 20072042), the State Key Program of Basic Research of China (grant 1998051115), Life Science Foundation for Young Scientists of CAS (grant STZ-00-06), Qi Ming Xing Foundation of Shanghai Ministry of Science and Technology (grant 00QB14034), and the Croucher Foundation. The calculations were performed on the SW-I supercomputer at the Shanghai Supercomputer Center.

REFERENCES

Bernstein, F. C., T. F. Koetzle, G. J. Williams, E. E. Meyer, Jr., M. D. Brice, J. R. Rodgers, O. Kennard, T. Shimanouchi, and M. Tasumi. 1977. The protein data bank: a computer-based archival file for macromolecular structures. *J. Mol. Biol.* 112:535–542.

Brooks, B. R., R. E. Bruccoleri, B. D. Olafson, D. J. States, S. Swaminathan, and M. Karplus. 1983. CHARMM: a program for macromolecular energy, minimization, and dynamics calculations. *J. Comp. Chem.* 4:187–217.

Brooks, C. L., I. I. I., and M. Karplus. 1983. Deformable stochastic boundaries in molecular dynamics. *J. Chem. Phys.* 79:6312–6325.

Brooks, C. L., I. I. I., M. Karplus, and B. M. Pettitt. 1988. Proteins: a theoretical perspective of dynamics, structure, and thermodynamics. *Adv. Chem. Phys.* 71:1–249.

Bryan, J. 1988. Gelsolin has three actin-binding sites. *J. Cell Biol.* 106: 1553–1562.

Burtnick, L. D., E. K. Koepf, J. Grimes, E. Y. Jones, D. I. Stuart, P. J. McLaughlin, and R. C. Robinson. 1997. The crystal structure of plasma gelsolin: implications for actin severing, capping, and nucleation. *Cell.* 90:661–670.

Chaponnier, C., P. A. Janmey, and H. L. Yin. 1986. The actin filament-severing domain of plasma gelsolin. *J. Cell Biol.* 103:1473–1481.

Grubmüller, H., B. Heymann, and P. Tavan. 1996. Ligand binding: molecular mechanics calculation of the streptavidin-biotin rupture force. *Science.* 271:997–999.

Israelewitz, B., M. Gao, and K. Schulten. 2001. Steered molecular dynamics and mechanical functions of proteins. *Curr. Opin. Struct. Biol.* 11: 224–230.

Jorgensen, W. L. 1981. Transferable intermolecular potential functions for water, alcohols, and ethers: application to liquid water. *J. Am. Chem. Soc.* 103:335–340.

Kwiatkowski, D. J. 1999. Functions of gelsolin: motility, signaling, apoptosis, cancer. *Curr. Opin. Cell Biol.* 11:103–108.

Kwiatkowski, D. J., P. A. Janmey, and H. L. Yin. 1989. Identification of critical functional and regulatory domains in gelsolin. *J. Cell Biol.* 108:1717–1726.

Kwiatkowski, D. J., T. P. Stossel, S. H. Orkin, J. E. Mole, H. R. Colten, and H. L. Yin. 1986. Plasma and cytoplasmic gelsolins are encoded by a single gene and contain a duplicated actin-binding domain. *Nature.* 323:455–458.

Lin, K. M., M. Mejillano, and H. L. Yin. 2000. Ca^{2+} regulation of gelsolin by its C-terminal tail. *J. Biol. Chem.* 275:27746–27752.

Lueck, A., H. L. Yin, D. J. Kwiatkowski, and P. G. Allen. 2000. Calcium regulation of gelsolin and adseverin: a natural test of the helix latch hypothesis. *Biochemistry.* 39:5274–5279.

McDonald, I. K., and J. M. Thornton. 1994. Satisfying hydrogen bonding potential in proteins. *J. Mol. Biol.* 238:777–793.

McGough, A. 1998. F-actin-binding proteins. *Curr. Opin. Struct. Biol.* 8:166–176.

Neria, E., S. Fisher, and M. Karplus. 1996. Simulation of activation energies in molecular systems. *J. Chem. Phys.* 105:1902–1921.

Pope, B. J., J. T. Gooch, and A. G. Weeds. 1997. Probing the effects of calcium on gelsolin. *Biochemistry.* 36:15848–15855.

Robinson, R. C., M. Mejillano, V. P. Le, L. D. Burtnick, H. L. Yin, and S. Choe. 1999. Domain movement in gelsolin: a calcium-activated switch. *Science.* 286:1939–1942.

Selden, L. A., H. J. Kinosian, J. Newman, B. Lincoln, C. Hurwitz, L. C. Gershman, and J. E. Estes. 1998. Severing of F-actin by the amino-terminal half of gelsolin suggests internal cooperativity in gelsolin. *Biophys. J.* 75:3092–3100.

Sun, H. Q., M. Yamamoto, M. Mejillano, and H. L. Yin. 1999. Gelsolin, a multifunctional actin regulatory protein. *J. Biol. Chem.* 274: 33179–33182.

Wallace, A. C., R. A. Laskowski, and J. M. Thornton. 1995. LIGPLOT: a program to generate schematic diagrams of protein-ligand interactions. *Protein Eng.* 8:127–134.

Way, M., and A. Weeds. 1988. Nucleotide sequence of pig plasma gelsolin: comparison of protein sequence with human gelsolin and other actin-severing proteins shows strong homologies and evidence for large internal repeats. *J. Mol. Biol.* 203:1127–1133.